

Research Paper

Calculation of the Dispersion Curves Modeling the Propagation of Ultrasonic Lamb Waves in a Bonded Aluminum/Epoxy/Aluminum Structure Using the Semi-Analytical Finite Element Method

Mustapha AZKOUR¹*, Mhammed EL ALLAMI²), Hassan RHIMINI¹)

¹) *Laboratory of Mechanics, Engineering, and Innovation
National High School of Electricity and Mechanics (ENSEM), Hassan II University
Casablanca, Morocco*

²) *Regional Center for Education and Training Professions (CRMEF)
Settat, Morocco*

*Corresponding Author e-mail: mustapha.azkour.doc22@ensem.ac.ma

The main aim of this paper is to calculate the dispersion curves modeling the propagation of ultrasonic Lamb waves inside a bonded tri-layer plane aluminum/epoxy/aluminum structure using the semi-analytical finite element (SAFE) method. The paper also aims to plot the nodal displacements normalized by their maximums for the four propagative modes that appear at the frequency of 200 kHz. These results contribute to the understanding of ultrasonic wave propagation in planar multilayer structures and have potential applications in non-destructive testing. The SAFE method is compared to the Graphical User Interface for Guided Ultrasonic Waves GUIGUW program. In general, this paper highlights the particular dispersive behavior of ultrasonic guided waves propagating in bonded three-layer structures. The GUIGUW program has been rarely utilized by authors to verify and compare results, particularly for this kind of structure, despite its robustness in calculating ultrasonic guided waves' dispersion curves. We are still among the few who have drawn this parallel. In this paper, we put forth a very clear-cut and accurate framework for determining the dispersion curves of a three-layer structure, and researchers who are new to the SAFE method may find this framework helpful as well. Another result shown in this paper is that the S0 mode is more sensitive to changes in the epoxy layer thickness than the A0 mode in the low-frequency range. Therefore, we can determine how much resin epoxy adhesive layer is missing from two ostensibly identical structures by estimating the difference in adhesive thickness. One of the structures is used as a reference, and the variation in phase velocity can allow the estimation of the lack of resin epoxy. However, if we want to assess defects such as debonding using the S0 mode, a low frequency should be used, and it must be strictly smaller than its frequency of high dispersivity and correspond to a maximum group velocity.

Keywords: non-destructive testing; bonded structures; ultrasonic guided waves; Lamb waves; semi-analytical finite element method; GUIGUW.

1. INTRODUCTION

If one compares bonding principles with other forms of assembly, such as welding, riveting, stapling, or bolting, one sees that bonding enables the combination of materials possessing quite diverse properties. These techniques guarantee assembly, whether it is permanent or removable. Like the assembly of car body pieces or empennages on aircraft cells, bonding can be either permanent or removable. Adhesive memory aids are good examples of removable bonding. In contrast, the mechanical assembly methods involve drilling the materials to be joined. In addition, the assembly effort is concentrated on these anchoring sites, causing localized stress on the surrounding structures. These stress localizations [1] are frequently the cause of splitting in one or both combined materials [2], potentially causing the constructed structure to collapse. It should also be noted here that in such assembly procedures, effective sealing is not guaranteed. All these assembly procedures have the benefit of being quick. As the bonding surface is often bigger than that produced by mechanical assembly, resulting in lower stresses for the same type of stress and reduced susceptibility to a fracture start that is always local. Bonding provides several advantages, including high strength, weight savings, the ability to integrate multiple materials of varied thicknesses, and convenience in combining complicated designs. While welding polymers for composites is only suitable for certain materials, adhesive bonding is progressively replacing mechanical assembly methods in the aerospace and automotive sectors. During commissioning, bonded structures may suffer damage caused by cyclic loading conditions or environmental conditions, leading to degradation of the adhesive layer. Therefore, a regular assessment of the state of the bonded joint is recommended. We were interested in non-destructive testing by ultrasonic guided waves of a structure assembled using bonding techniques, because this method is very sensitive to changes in size, position, and mechanical properties of the interfaces between different layers [3].

THOMSON [4] and HASKELL [5] conducted theoretical studies on the transmission of a plane elastic wave through a stratified solid, consisting of any number of plates of different materials and thicknesses by using the matrix method to systematize the analysis and present equations in a form suitable for computation. SEIFRIED [6] integrated an analytic model, the finite element method, and experimental measures to gain a quantitative understanding of the dispersion features of guided Lamb waves in multilayered adhesive-bonded components. LINDGREN *et al.* [7] presented the inspection of defects in multilayer structures using high frequency ultrasonic guided waves. The obtained results proved a substantial reduction in the pervasion of ultrasonic guided waves at high frequencies when an adhesive material was present between the layers. LOWE and COWLEY [8] investigated the possibility of applying plate waves to assess the health

of adhesive joints and reviewed modal techniques that could be used to measure the adhesion and cohesion properties of adhesive joints.

ROKHLIN [9] conducted a theoretical and experimental analysis of the interaction of Lamb waves with lap-shear joints. Additionally, LOWE *et al.* [10] investigated the transmission of Lamb waves across adhesively bonded lap joints using finite element analysis. The study considered three modes for excitation and reception (S0, A0, and A1) applied to lap joints consisting of parallel aluminum sheets bonded with an epoxy adhesive. In the last few decades, many non-destructive studies have been developed. For example, WANG *et al.* [11] proposed a framework for the detection and sizing of disbonds in a multilayer bonded structure using modally selective guided wave experiments both in actual experiments and numerical simulations. Both numerical and experimental validations were performed, in which disbonds of different lengths, ranging from 10 to 40 mm, were examined.

GAUTHIER *et al.* [12] presented a method for characterizing the level of adhesion in structural metal/adhesive/metal bonding using ultrasonic guided waves and showed that the cut-off frequency measurement of the vertical longitudinal mode can be a very good indicator of bonding integrity. Several numerical methods have been used to determine the dispersion curves of tri-layer and multilayer structures. The precise calculation of dispersion curves is a crucial preliminary step in non-destructive testing using ultrasonic guided waves. For example, ZITOUNI *et al.* [13] proposed a novel hybrid analytical algorithm to calculate the dispersion curves in multilayer plane structures. Their algorithm achieved good convergence and shorter computation times by combining the bisection and Newton-Raphson techniques. In another paper, ZITOUNI *et al.* [14] used the spectral method to study the propagation of ultrasonic guided waves in a graphite-epoxy composite plate. They calculated dispersion curves for various fiber orientations, and compared their results with those obtained from the DISPERSE software. In order to determine the dispersion curves of ultrasonic guided waves in anisotropic media, ZITOUNI *et al.* [15] compared several methods. They particularly contrasted their results with those of NAYFEH and CHIMENTI [16]. The dispersion curves were calculated for a wide range of structures by using an implementation of finite element models [17], ensuring accurate mode prediction due to element discretization.

DENG *et al.* [18] developed a simplified model of bi-layer composite insulators using the theory of ultrasonic guided wave propagation. To address the issue of composite insulator debonding, they analyzed the propagation velocity and energy decay of longitudinal and torsional ultrasonic guided waves in the insulator bilayer model. Based on the ultrasonic guided wave attenuation characteristics, they proposed a method for detecting axial and circumferential debonding of composite insulators. BOUGAZE *et al.* [19] investigated ultra-

sonic guided waves in a tri-layer structure consisting of two aluminum sheets bonded by a resin epoxy adhesive layer. They also showed how the quality of bonding could be determined by examining the dispersion curves. To investigate a novel use of ultrasonic Lamb waves for detecting the coating disbond in an aluminum-adhesive double-layer waveguide and a triple-layer waveguide (aluminum-adhesive-coating), MEHRABI *et al.* [20] carried out experimental and numerical studies. The purpose of their experimental tests was to determine how the adhesive bonding influences the attenuation of Lamb waves in addition to the coating layer's influence on Lamb wave behavior.

In the current study, we are interested in studying the propagation of ultrasonic Lamb waves in planar multilayer structures to trace the dispersion curves and possibly for non-destructive evaluation. So, we study the propagation of ultrasonic Lamb waves in a planar tri-layer bonded aluminum/epoxy/aluminum structure, and we use the semi-analytical finite element (SAFE) [21, 22] method to calculate dispersion curves and nodal displacements. Next, we compare them with those obtained by using Graphical User Interface for Guided Ultrasonic Waves (GUIGUW), a widely-used commercial program for analyzing ultrasonic guided wave propagation in elastic media. Our research contributes to understanding the dispersion properties of ultrasonic Lamb waves in planar multilayer structures, holding potential usage in applications in non-destructive evaluation. Additionally, our study reveals that the S0 mode is more sensitive to changes in epoxy layer thickness than the A0 mode, especially in the low-frequency range.

2. OVERVIEW OF THE SEMI-ANALYTICAL FINITE ELEMENT METHOD (SAFE)

2.1. Tri-layer plane structure sample

To calculate the dispersion curves modeling the propagation of ultrasonic guided waves in our planar tri-layer structure (aluminum/epoxy/aluminum) using the semi-analytical finite element SAFE method, a sample of the structure is presented with all the mechanical and geometric properties shown below (see Fig. 1 and Table 1).

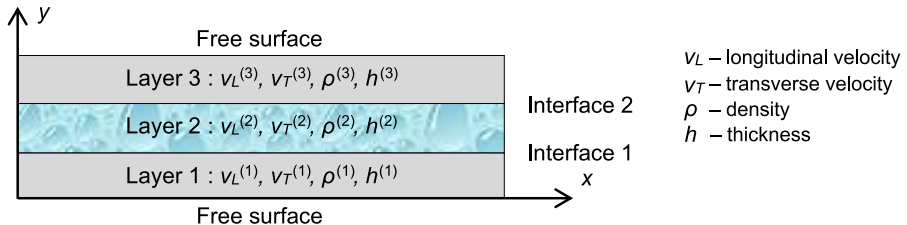


FIG. 1. Geometric configuration of the planar tri-layer structure.

Table 1. Mechanical and geometric properties of the planar tri-layer structure.

Layer	Material	Longitudinal velocity [m/s]	Transverse velocity [m/s]	Density [kg/m ³]	Thickness [mm]
1	Aluminum	6150	3100	2700	3
2	Epoxy	771	370	1106	0.25
3	Aluminum	6150	3100	2700	3

2.2. Theoretical formulation

The calculation of dispersion curves is based on the following presumptions:

- 1) Each layer is regarded as a homogeneous, elastic, and isotropic medium.
- 2) The faces of the tri-layer structure are free from constraints.
- 3) Based on Hamilton's principle, the computation will be developed.
- 4) The Gaussian quadrature method will be used to approximate the elementary stiffness and mass matrices.

The dispersion curves for any planar tri-layer structure can be calculated using the SAFE method, which combines the finite element method with analytical expressions. In this study, we consider a planar bonded tri-layer aluminum/epoxy/aluminum structure with infinite width. So, the model simplifies to a 2D problem in the x - y plane with an ultrasonic guided wave propagating along the x -direction (see Fig. 2), and the cross-section domain is divided into a system of 2D elementary layers, modeled using 1D finite elements with three nodes, as shown below.

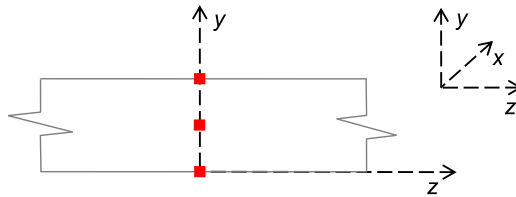


FIG. 2. Infinite 2D elementary layer with three nodes [21, 22].

Using the Hamilton principle [21], the equation of motion for the cross-section in its linear form can be written as follows:

$$(2.1) \quad (\mathbf{A} - \omega^2 \mathbf{M}) \mathbf{Q} = \mathbf{0},$$

where

$$(2.2) \quad \mathbf{A} = \mathbf{K}_1 + k \widehat{\mathbf{K}}_2 + k^2 \mathbf{K}_3, \quad \mathbf{Q} = \begin{bmatrix} \widehat{\mathbf{U}} & k \widehat{\mathbf{U}} \end{bmatrix}^T.$$

Here, $\omega = 2\pi f$ represents angular frequency, k denotes the wavenumber, \mathbf{T} is the symbol for matrix transpose, and [22]

$$(2.3) \quad \mathbf{M} = \bigcup_{e=1}^{N_{el}} \mathbf{m}^{(e)}, \quad \mathbf{K}_n = \bigcup_{e=1}^{N_{el}} \mathbf{k}_n^{(e)}, \quad n = 1, 2, 3,$$

where N_{el} denotes the number of elements. $\widehat{\mathbf{K}}_2$ and $\widehat{\mathbf{U}}$ represent the \mathbf{K}_2 symmetric real matrix and the cross-sectional mode shape or the new displacement vector, respectively. For any frequency obtained by solving Eq. (2.1), the phase velocity V_P and the wavelength λ can be deduced using the following formulas:

$$(2.4) \quad V_P = \omega/k,$$

and

$$(2.5) \quad \lambda = 2\pi/k.$$

Furthermore, Eq. (2.1) leads to calculating the group velocity V_G as follows:

$$(2.6) \quad V_G = \frac{\partial \omega}{\partial k} = (\boldsymbol{\phi}_R^T \mathbf{K}' \boldsymbol{\phi}_R) / (2\omega \boldsymbol{\phi}_R^T \mathbf{M} \boldsymbol{\phi}_R),$$

where $\boldsymbol{\phi}_R$ denotes the right eigenvector of the system and \mathbf{K}' is defined by:

$$(2.7) \quad \mathbf{K}' = \widehat{\mathbf{K}}_2 + 2k\mathbf{K}_3.$$

2.3. Numerical solution

To compute dispersion curves, we study the dispersion characteristics of ultrasonic guided waves in planar multilayer structures. Thus, we present a framework that outlines the key stages involved in developing a Matlab code that can compute the dispersion curves and nodal displacements for any planar multilayer structure through the application of the SAFE method (refer to Fig. 3).

2.4. Dispersion curves of the three-layer structure

2.4.1. Determination of the minimum number of elements N_{\min} . The framework discussed above was implemented efficiently in the Matlab language and the resulting code was executed. This code allowed us to plot the dispersion curves (see Subsec. 2.4.3, Figs. 9–12). It should be noted that for each frequency range, there is a well-defined number of modes, and for all these modes to appear in the figures, it is necessary to determine the minimum number of elements N_{\min} from which the maximum number of modes is reached. So, if we consider the frequency range of 3 MHz, determining the number of possible modes necessitates knowledge of N_{\min} . One can vary the number of elements up to a sufficiently large value and record the number of generated modes. In fact,

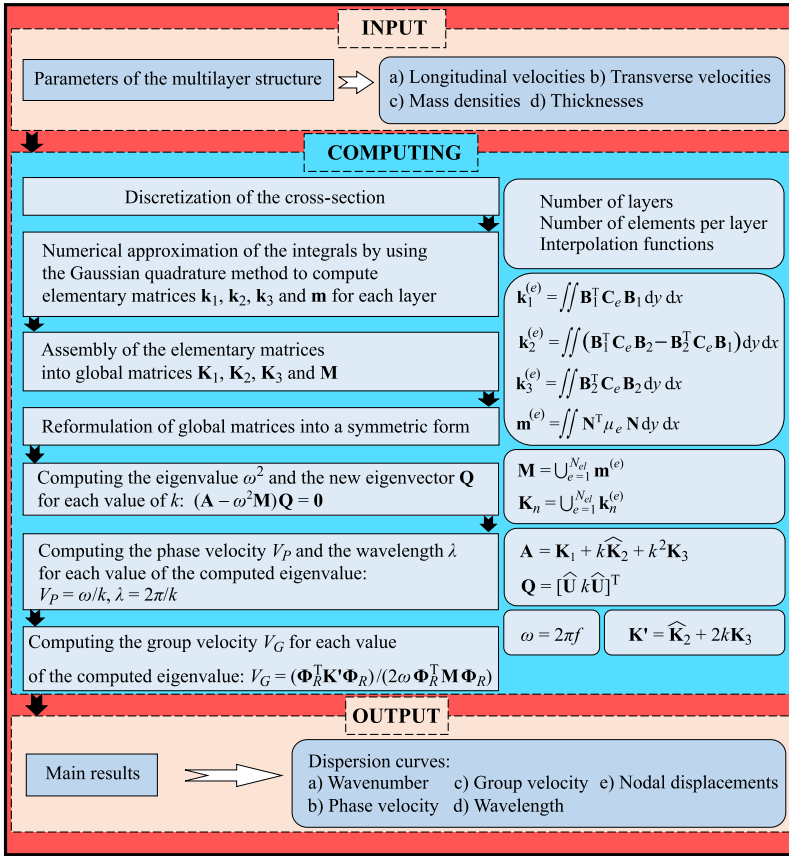


FIG. 3. Framework for calculating the dispersion curves and nodal displacements using SAFE.

one can create a numerical sequence $N_m = f(N_{el})$ by assigning to each number of elements N_{el} the corresponding number of all modes N_m , as shown in Table 2.

Table 2. The number of elements determines how many modes appear in the 3 MHz frequency range.

N_{epl}	N_{el}	N_{osm}	N_{oam}	N_m
1	3	7	7	14
2	6	10	10	20
3	9	10	10	20
4	12	12	11	23
5	15	12	11	23
6 to 120	18 to 360	12	12	24

N_{epl} is the number of elements per layer, N_{el} is the number of elements, N_{osm} is the number of symmetric modes, N_{oam} is the number of antisymmetric modes, N_m is the number of modes.

From Table 2, we can deduce that the number of all possible modes that can appear in the frequency range of 3 MHz is equal to 24 with 12 symmetric modes and 12 antisymmetric modes. This occurs when the number of elements per layer varies from 6 up to 120. This will surely keep its value when $N_{epl} \geq (120 + n)$ for every integer $n \geq 1$. Therefore, it is evident that N_{\min} is equal to 18.

2.4.2. The influence of the number of elements on the number of modes appearing. For each given frequency range, there exists a maximum number of modes that must appear. Corresponding to this maximum, there is a minimum number of elements with which the calculation of the dispersion curves must be made. This is the subject of this subsection (see Figs. 4–8).

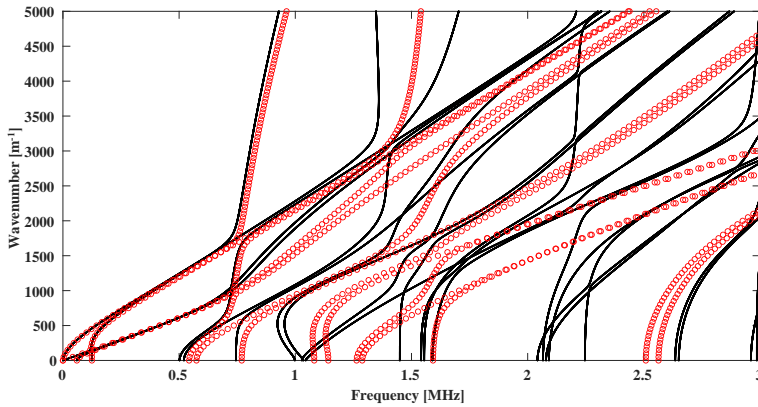


FIG. 4. Wavenumber dispersion curves by SAFE: red circles for $N_{el} = 3$ vs. black points for $N_{el} = 18$.

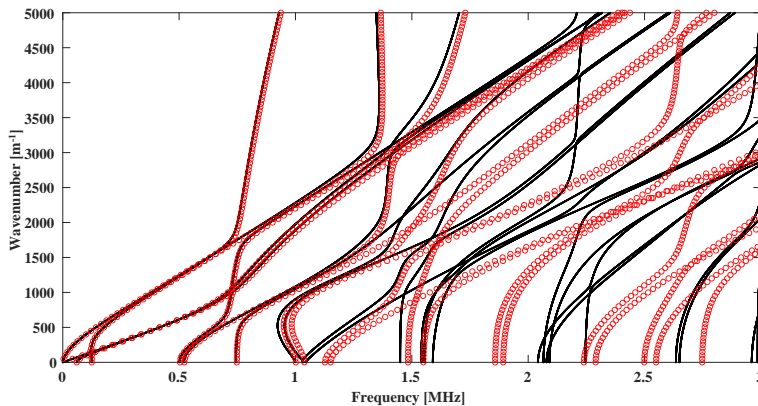


FIG. 5. Wavenumber dispersion curves by SAFE: red circles for $N_{el} = 6$ vs. black points for $N_{el} = 18$.

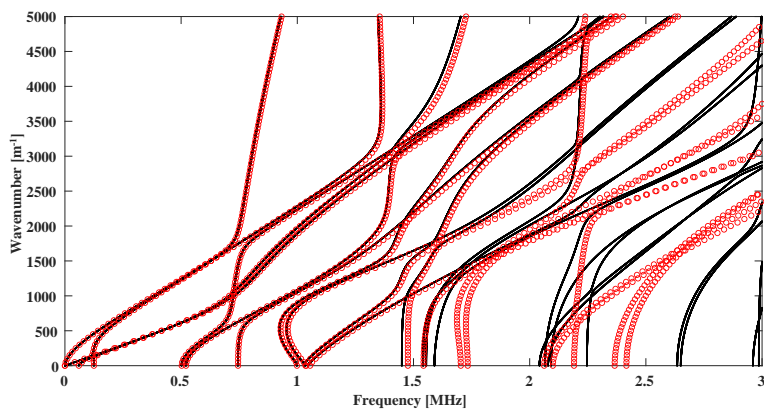


FIG. 6. Wavenumber dispersion curves by SAFE: red circles for $N_{el} = 9$ vs. black points for $N_{el} = 18$.

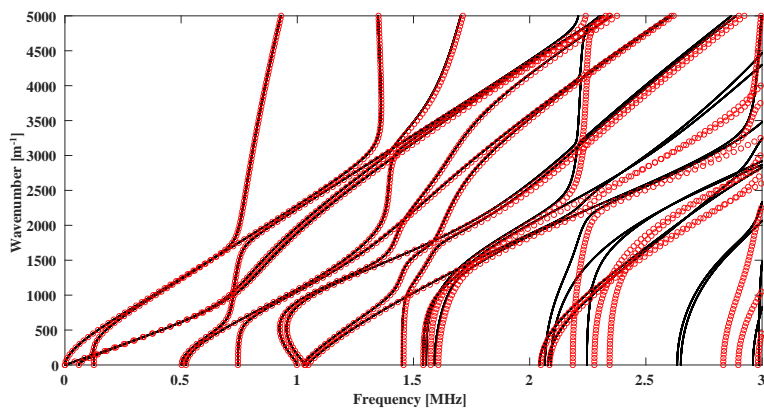


FIG. 7. Wavenumber dispersion curves by SAFE: red circles for $N_{el} = 12$ vs. black points for $N_{el} = 18$.

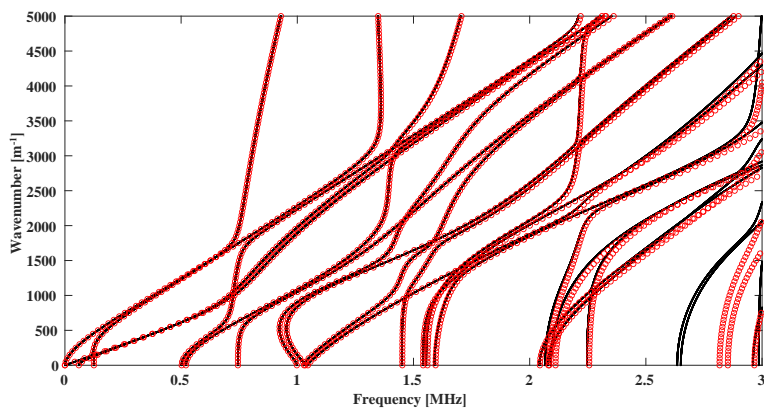


FIG. 8. Wavenumber dispersion curves by SAFE: red circles for $N_{el} = 15$ vs. black points for $N_{el} = 18$.

The number of elements chosen in this study is a multiple of 3, such that each layer has the same number of elements. When the number of elements N_{el} is 3 (as shown in Fig. 4), 14 modes appear in a frequency range of 3 MHz. Among these 14 modes, only the first four modes align adequately with the expected modes for $N_{el} = 18$ within a restricted frequency range. We can see that 14 is always less than the maximum number of expected modes, which is 24, in the same frequency range. For $N_{el} = 6$ (as shown in Fig. 5), the number of modes appearing increases from 14 to 20. The number of modes coinciding with the expected modes when $N_{el} = 18$ also increases from 4 to 7, and the frequency range of this coincidence expands. Furthermore, 20 is lower than the maximum number of expected modes – 24, in the frequency range of 3 MHz. For $N_{el} = 9$ (see Fig. 6), where 20 modes appear, the number of coinciding modes with $N_{el} = 18$ increases from 7 to 11, along with an expanded frequency range of coincidence for the first 7 modes. For $N_{el} = 12$ (see Fig. 7), the number of modes is 23, with 13 modes coinciding with those of $N_{el} = 18$. Similarly, for $N_{el} = 15$ (see Fig. 8), the number of modes is 23. So, N_{\min} must be higher than 15, and numerical verification shows that the minimum number of elements should be equal to 18 when each layer has the same number of elements. If each layer is divided into a different number of elements, it is necessary to perform another numerical calculation to determine if N_{\min} differs from 18. It is noticed that the coincidence of the modes appearing obtained by increasing the number of elements takes place and it is prolonged on the left side of the frequency range. The precision of dispersion curves calculated by the SAFE method depends on the chosen number of elements. So, for each desired precision in each frequency range, it is necessary to determine the number of elements for which this precision will be well ensured. Thus, for a desired precision p_0 , we cannot be sure that the calculated N_{\min} will ensure the accuracy in the same frequency range.

Determining the minimum number of elements N_{\min} by varying the number of elements N_{el} , as presented in Table 2, has been crucial, as we did not find any precise formula in the literature making it possible to determine N_{\min} for any given frequency range in the case of a three-layer bonded structure. However, for a single plate, GALÁN and ABASCAL [23] provided a precise formula. Nevertheless, this study visualizes the satisfactory coincidence of lower order modes, particularly A0 and S0 modes, calculated with $N_{el} = N_0 = 3$, to which we can add A1 and S1 with those calculated by N_{\min} , provided that the upper limit of the chosen frequency band does not exceed a certain relatively low value. Finding a formula to determine N_{\min} directly for bonded three-layer structures can be the subject of another paper. We must remember that if the number of elements increases, then the following remarks hold:

- a) The number of modes increases.
- b) The precision of solutions improves.
- c) The computing time increases.
- d) High-performance computing hardware is required, etc.

2.4.3. Plotting the dispersion curves using the minimum number of elements. The dispersion curves presented below (Figs. 9–12) are calculated using N_{\min} .

The number and types of modes (symmetric and antisymmetric) that can propagate in the structure at various frequencies are depicted in Fig. 9. However, when we are forced to use signal processing in an experimental or numerical

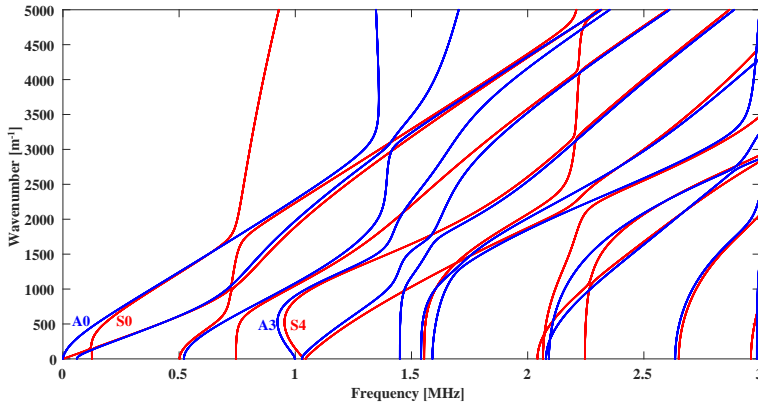


FIG. 9. Wavenumber dispersion curves of the planar tri-layer aluminum/epoxy/aluminum structure.

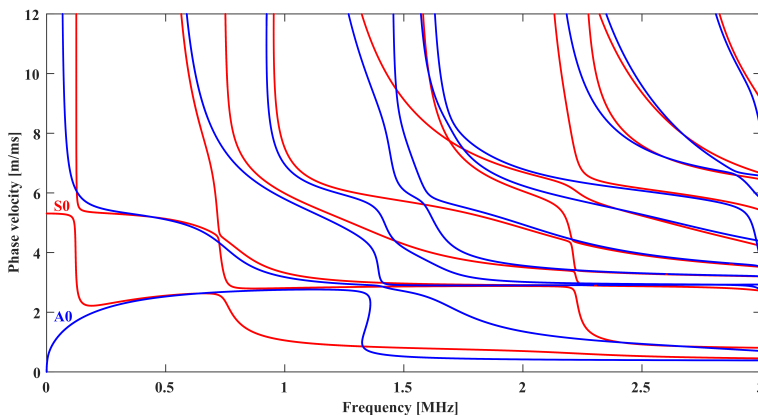


FIG. 10. Phase velocity dispersion curves of the planar tri-layer aluminum/epoxy/aluminum structure.

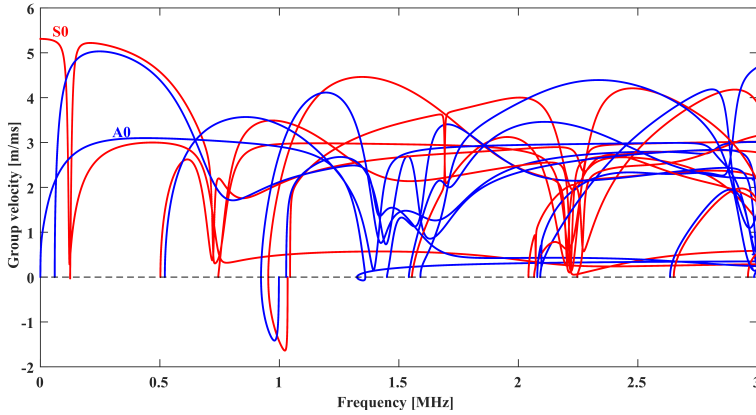


FIG. 11. Group velocity dispersion curves of the planar tri-layer aluminum/epoxy/aluminum structure.

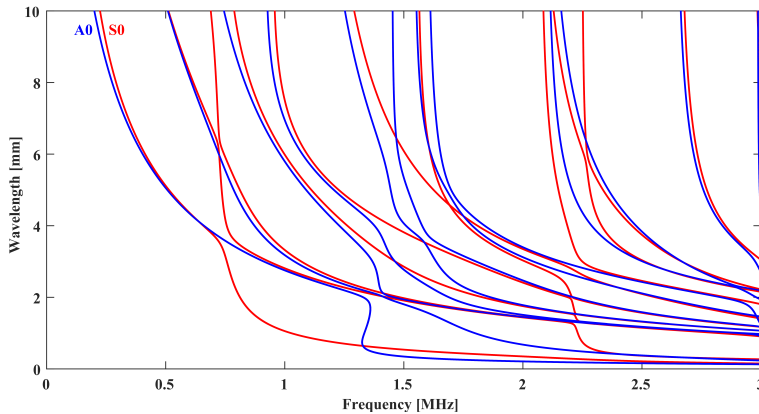


FIG. 12. Wavelength dispersion curves of the planar tri-layer aluminum/epoxy/aluminum structure.

study of the interaction of ultrasonic guided waves with one or more defects in such a structure, we want to minimize the number of modes that can propagate. Since A0 and S0 are fundamental and always exist regardless of the excitation frequency, this count can no longer be less than two.

Comparing an isotropic structure of the same thickness with a bonded structure reveals that the latter has a comparatively higher number of propagating modes. Our three-layer structure is a dispersive medium, as evidenced by the wavenumber curves' lack of rectilinear lines. Nonetheless, the variation is nearly linear for some frequency ranges, which may indicate a less dispersive nature. Examining the wavenumber curves, for instance, in the 0–0.1 MHz frequency range, the S0 mode exhibits very weak dispersive behavior. It is evident that at certain frequencies, symmetric and antisymmetric modes intersect, and there

exist frequency ranges where two distinct modes are so close to each other that they appear to be asymptotes of each other. We believe that this effect is most likely caused by the adhesive layer. Each one of the two modes, A3 and S4, can have two distinct wavenumbers for the same frequency, approximately 1 MHz. There are then two group velocities with the opposite signs, indicating that a wave packet with a negative group velocity travels against the direction of propagation.

Except for the modes A0 and S0, with cutoff frequencies at 0 and the corresponding phase velocities being noninfinite, the vertical lines whose abscissa are the cutoff frequencies of the symmetric and antisymmetric modes are vertical asymptotes for the phase velocity curves. Equations (2.4) and (2.6) lead us to the conclusion that:

$$(2.8) \quad V_G = V_P^2 \left(V_P - f \frac{\partial V_P}{\partial f} \right)^{-1}.$$

It is then important to note that the group velocity and the frequencies corresponding to the extrema of the phase velocity are the same, and this equality is well-known in non-dispersive media ($V_G = V_P$). We observe that there are likely a few frequencies with three-phase velocities in the 1.25–1.5 MHz band for the A0 mode.

The associated group velocities are zero or almost zero when the wavenumber curves for nearby frequencies appear vertical or nearly vertical. Certain frequencies result in too low or zero group velocities. Therefore, selecting these frequencies for excitation would not be a good idea if we wanted to conduct experimental or numerical studies on three-layer structures because it would require a large execution time and the need for quite powerful resources. Notably, the phase velocity is substantially higher near the cutoff frequencies than the group velocity, even with a certain increase in velocity. By comparing the group velocity with the phase velocity, we notice that the latter is higher. We know that the relationship between the wavenumber and the group velocity is given by:

$$(2.9) \quad V_G = 2\pi \left(\frac{\partial k}{\partial f} \right)^{-1}.$$

As a result, the group velocity in a frequency band where the wavenumber varies linearly is constant; this is evident for the S0 mode in the 0–0.1 MHz band.

The vertical asymptotes for the wavelength curves are the lines whose abscissas are the cutoff frequencies of the symmetric and antisymmetric modes. A higher frequency corresponds to a shorter wavelength. The wavelength does, however, decrease for the A0 mode, but at a certain point, it moves backward in a zigzag pattern (see Fig. 12), creating the potential for two distinct wavelengths for the same frequency. It should be mentioned that determining the

wavelength is crucial when utilizing the finite element method to simulate and investigate how ultrasonic guided waves interact with a defective three-layer structure.

2.5. SAFE method compared to GUIGUW program

2.5.1. Comparison of dispersion curves. The dispersion curves calculated by the SAFE method and those obtained by the GUIGUW program are compared using N_{\min} .

The dispersion curves obtained using the SAFE method and those calculated using the GUIGUW program show good agreement, as shown in Figs. 13–16. The solutions determined by the GUIGUW program and the SAFE method, under

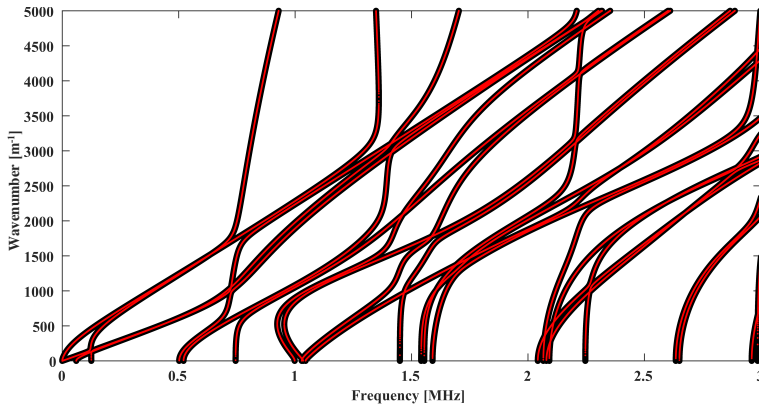


FIG. 13. Superposition of k -dispersion curves: red points by GUIGUW vs. black circles by SAFE.

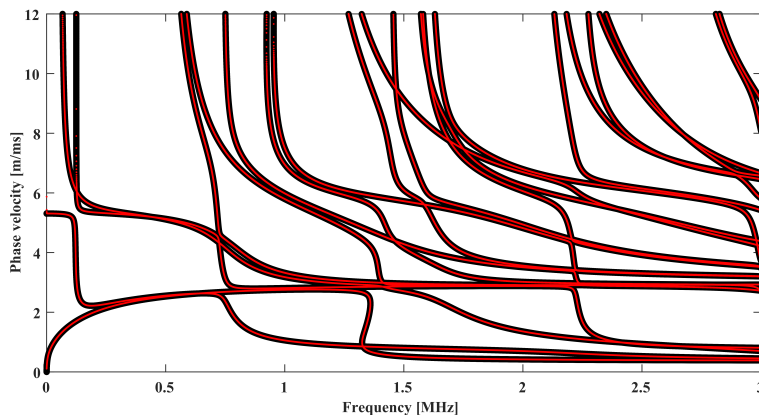


FIG. 14. Superposition of V_P -dispersion curves: red points by GUIGUW vs. black circles by SAFE.

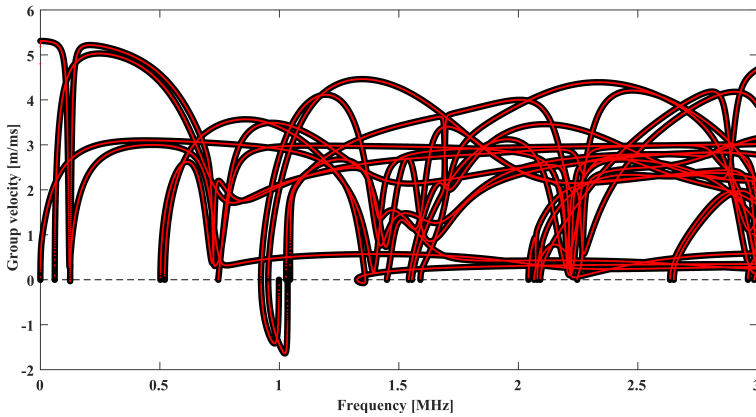


FIG. 15. Superposition of V_G -dispersion curves: red points by GUIGUW vs. black circles by SAFE.

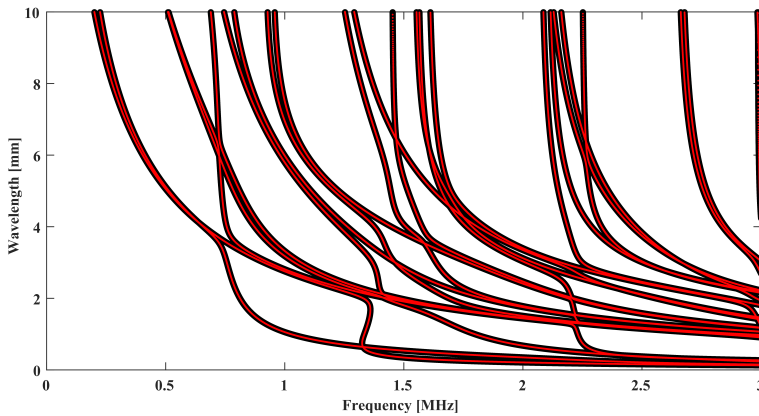


FIG. 16. Superposition of λ -dispersion curves: red points by GUIGUW vs. black circles by SAFE.

the previously outlined framework approach, are perfectly aligned in Figs. 13–16. To keep the GUIGUW or SAFE curves from being obscured by the others, we had to trace the solutions in extremely bold black circles. This shows the perfect coincidence between the SAFE method and the GUIGUW program. Calculating a relative error or difference between GUIGUW and SAFE was not possible due to their perfect coincidence. In light of this, we can conclude that, by selecting the f -fixed approach, the GUIGUW program most likely operates using the SAFE method. Additionally, the GUIGUW curves indicate that there are frequency regions in which the solutions deviate significantly, a phenomenon not observed in our SAFE code. It is important to note that we employed the same number of elements per layer as in the GUIGUW program.

2.5.2. Comparison of displacements. We chose to compute the longitudinal displacements \mathbf{u}_x and transverse displacements \mathbf{u}_y using the SAFE method at the frequency $f = 200$ kHz. Then, we find that at this frequency, two symmetric modes S0 and S1 and two antisymmetric modes A0 and A1 are observed (see Fig. 17).

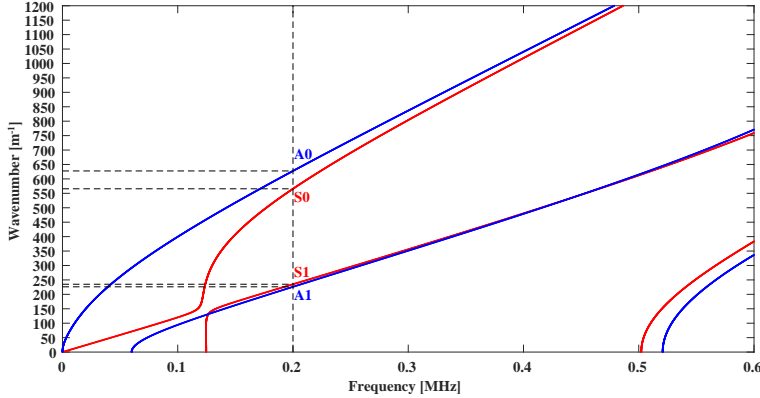


FIG. 17. Appearing Lamb modes at the frequency of 200 kHz.

Table 3. Wavenumbers, phase velocities, group velocities, and wavelengths for A0, S0, A1, and S1 at the frequency of 200 kHz.

Mode	Wavenumber [1/m]	Phase velocity [m/s]	Group velocity [m/s]	Wavelength [mm]
A0	627.592	2002.313	2927.364	10.011
S0	565.748	2221.194	2340.726	11.105
A1	226.090	5558.105	4998.748	27.790
S1	235.021	5346.900	5217.721	26.734

According to the SAFE method, the nodal displacement is given by:

$$(2.10) \quad \mathbf{u} = [\mathbf{u}_x \quad \mathbf{u}_y]^T = [i\mathbf{U}_x \quad \mathbf{U}_y]^T e^{i(kx - \omega t)}$$

with $\omega = 2\pi f$, \mathbf{U}_x and \mathbf{U}_y are the real amplitudes of the nodal displacements \mathbf{u}_x and \mathbf{u}_y , respectively, and these amplitudes are represented for all four modes in Figs. 18–21. The displacements calculated by the SAFE method and those obtained by the GUIGUW program are compared using N_{\min} .

The normalized displacement curves calculated using the SAFE method and those obtained using the GUIGUW program show good agreement, as shown in Figs. 18–21. The GUIGUW program provides displacements in the range of -1 to 1 . We normalized our displacements by their absolute maximum values to facilitate comparisons between our displacements and those of the GUIGUW

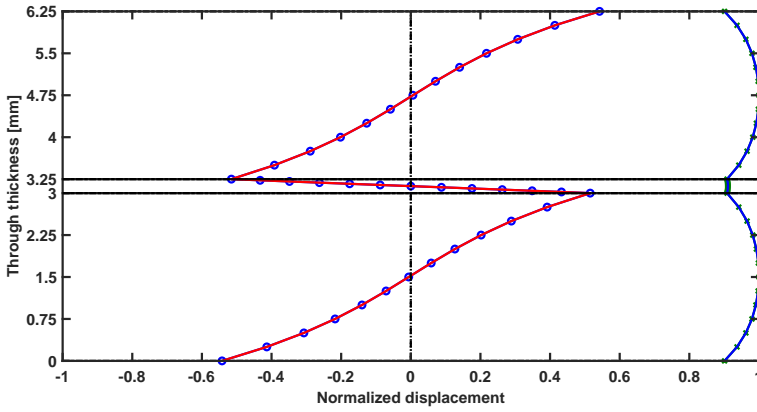


FIG. 18. Normalized displacements \mathbf{u}_x and \mathbf{u}_y at $f = 200$ kHz for the A0 mode: red (\mathbf{u}_x) and blue (\mathbf{u}_y) solid lines by the SAFE method vs. blue circles and green cross by the GUIGUW program.

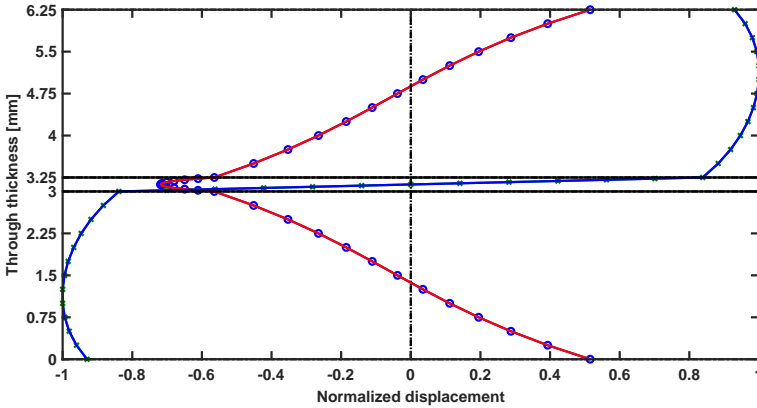


FIG. 19. Normalized displacements \mathbf{u}_x and \mathbf{u}_y at $f = 200$ kHz for the S0 mode: red (\mathbf{u}_x) and blue (\mathbf{u}_y) solid lines by the SAFE method vs. blue circles and green cross by the GUIGUW program.

program. The nodal displacements provided by the SAFE method are typically of the order of 10^{-4} or 10^{-5} . For both SAFE and GUIGUW, the same number of elements per layer is considered. We can see that all modes' displacements are continuous. When a mode is symmetric, its normal displacements are antisymmetric concerning the structure's median plane, but its longitudinal displacements are symmetric. Antisymmetric modes exhibit the opposite behavior. Another finding for antisymmetric modes is that, under excitation, the point in the structure's median plane does not move longitudinally ($u_x = 0, u_y \neq 0$); in contrast, for symmetric modes, it is limited to the longitudinal movement ($u_x \neq 0, u_y = 0$).

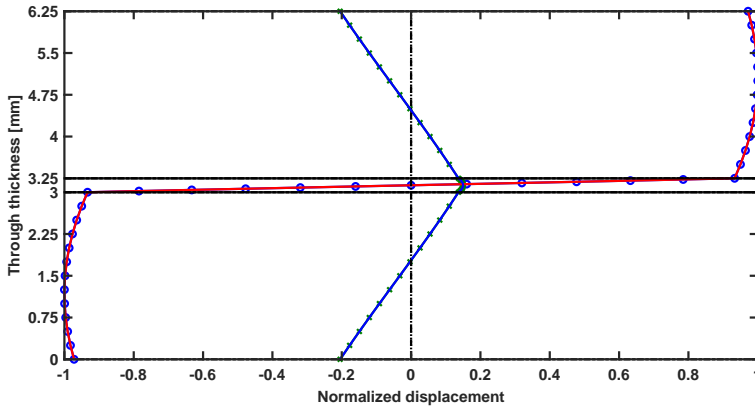


FIG. 20. Normalized displacements \mathbf{u}_x and \mathbf{u}_y at $f = 200$ kHz for the A1 mode: red (\mathbf{u}_x) and blue (\mathbf{u}_y) solid lines by the SAFE method vs. blue circles and green cross by the GUIGUW program.

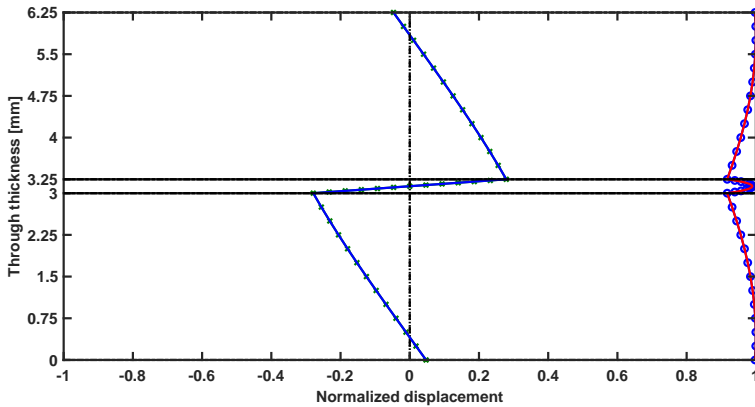


FIG. 21. Normalized displacements \mathbf{u}_x and \mathbf{u}_y at $f = 200$ kHz for the S1 mode: red (\mathbf{u}_x) and blue (\mathbf{u}_y) solid lines by the SAFE method vs. blue circles and green cross by the GUIGUW program.

2.5.3. Choice of location for testing. In this section, we seek to determine the best frequency that can ensure good testing by limiting the choice to the fundamental modes A0 and S0 (see Figs. 22 and 23). As a matter of fact, in bonded three-layer structures, certain modes exhibit greater sensitivity to variations in adhesive thickness, and these can be either symmetric or antisymmetric modes. To determine which of the modes would be more sensitive, though, if we were to restrict the options to the fundamental modes A0 and S0, the following will address this query.

A better location for testing would be where quantity $\Delta V_P/V_P$ is substantial. So, the obvious choice is the S0 mode, occurring at around $f = 0.12$ MHz, and

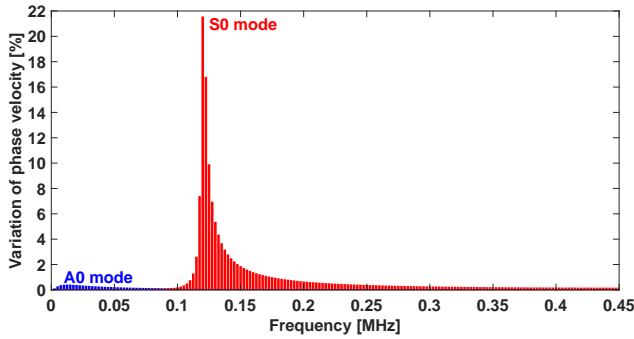


FIG. 22. The variation in the phase velocity $\Delta V_P/V_P$ when the thickness of the epoxy layer is increased by 5% for the A0 mode and the S0 mode.

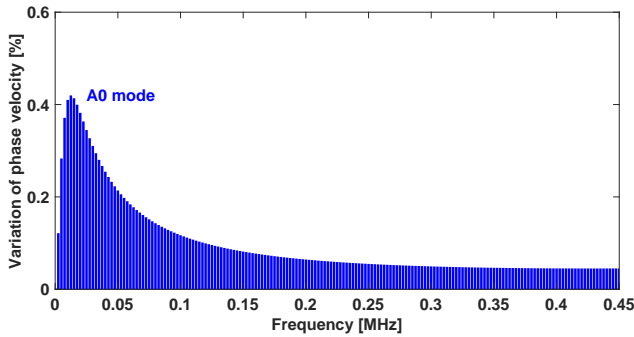


FIG. 23. Zoom at the variation in the phase velocity $\Delta V_P/V_P$ when the thickness of the epoxy layer is increased by 5% for the A0 mode.

$\Delta V_P/V_P = 21.56676221\%$, as shown in Fig. 22. However, at this frequency, the quantity $\Delta V_P/V_P$ is very small, reaching 0.099315001% for the A0 mode, and its maximal value across the range of 0.45 MHz does not exceed 0.419707654% at around $f = 0.0125$ MHz. Regrettably, the sensitivity of the S0 mode is higher, but it is situated in its most dispersive domain. So, if someone is interested in estimating the thickness of the adhesive layer or the absence of epoxy resin in this kind of structure, we can advise them to use the S0 mode for exciting a real structure or numerical sample because the S0 mode will provide more information about estimating the thickness of epoxy or the lack of epoxy. However, for detecting and sizing disbonds, for example, it is advised to aim for a maximum group velocity and a frequency that shows minimal dispersive behavior. So, using the $0\text{--}0.1$ MHz band is strongly recommended for the present structure.

To observe the impact of the variation in epoxy thickness on the S0 mode's phase and group velocities, we selected its high dispersivity frequency, or roughly 0.12 MHz (see Figs. 24 and 25).

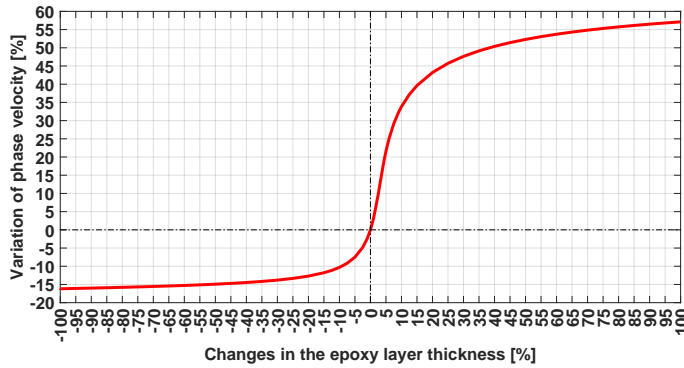


FIG. 24. The quantity $\Delta V_P/V_P$ in relation to the variation in the epoxy layer thickness for the S0 mode at the frequency $f = 0.12$ MHz.

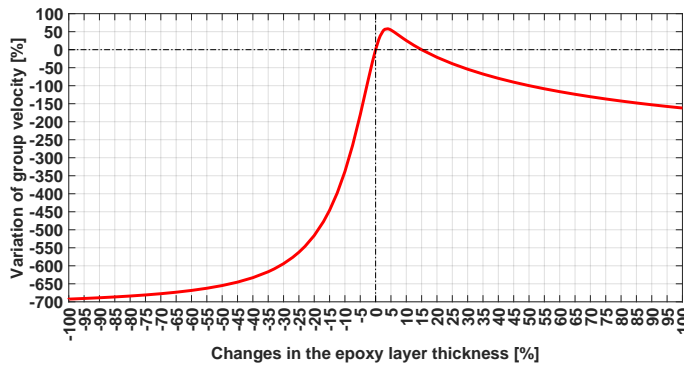


FIG. 25. The quantity $\Delta V_G/V_G$ in relation to the variation in the epoxy layer thickness for the S0 mode at the frequency $f = 0.12$ MHz.

We observed that an increase in epoxy layer thickness leads to a decrease in phase velocity, and vice versa. However, an equal amount of epoxy added or removed does not always translate into an equal phase velocity variation. In other words, the curve indicates that the function is no longer odd, as seen in the values for the positive abscissa being significantly higher than those for the negative abscissa. Epoxy is a material that encourages slowness in a way. We can say that this variation of phase velocity follows hysteretic behavior.

The first thing that immediately stands out in the above figure is that, unlike the phase velocity variation shown in Fig. 24, the group velocity variation does not follow the same pace. However, this time, the variations are more significant; for instance, a 5% change in epoxy thickness results in a velocity change of 54.6139%, while the phase velocity variation does not exceed 21.5667%. The figure clearly shows more representative values. The group velocity tends to in-

crease for most of the thickness range considered; however, this increase is more pronounced when the epoxy thickness decreases compared to when it increases. The group velocity only decreases when the thickness increases by a percentage of no more than 15%.

For group velocity only, at a low frequency of $f = 1$ kHz, the variation is measured as given in Fig. 26.



FIG. 26. The quantity $\Delta V_G/V_G$ in relation to the variation in the epoxy layer thickness for the S0 mode at the frequency $f = 10^{-3}$ MHz.

Figure 26 shows that for the S0 mode with a fixed frequency of 1 kHz, neither a significant change in the epoxy layer thickness nor a decrease in it results in the group velocity variation. The group velocity associated with this frequency is roughly equal to the top velocity for the S0 mode. We note that the group velocity variation is represented by an affine function. The following hypothesis can be supported by the negligible change in group velocity that occurs in response to changes in the thickness of the epoxy layer: it is advised to inspect a structure bonded by the S0 mode at low frequencies, preferably at a frequency that corresponds to a value near the maximum value of the group velocity, as this parameter may not have any bearing on the sensitivity of experimental results, especially when looking for a defect in the epoxy layer.

3. RESULTS AND DISCUSSION

The dispersive behavior of ultrasonic guided waves propagating in a three-layer structure was demonstrated in this paper, along with the frequencies at which this behavior is most noticeable. We chose and established the frequency range in this paper to study the interaction of ultrasonic guided waves with a defect in a bonded three-layer structure. Key findings are as follows:

- 1) Our research demonstrates how the GUIGUW program employs the SAFE method. But the strategy we employ in this paper ensures that the desired

solutions are not overlooked. One advantage of the k -fixed method we used is this: the f -fixed approach used by the GUIGUW program increases the likelihood of missing solutions, especially when the wavenumber represents vertical or nearly vertical curve segments. However, the f -fixed approach may have the advantage of a faster calculation time.

- 2) This paper shows that because the S0 mode is more sensitive to changes in the adhesive layer thickness, it is the ideal candidate for excitation in the identification and evaluation of adhesive layer deficiency. The phase velocity is unnecessarily large near cutoff frequencies and the cutoff frequency modifies slightly in response to variations in the thickness of the adhesive layer. This paper recommends the following tasks: We can choose the S0 mode to determine whether a real-bonded three-layer structure has the same adhesive layer thickness as the theoretical sample.
- 3) Let us emphasize that each frequency range has a fixed number of modes and that the minimum number of elements from which the maximum number of modes is reached must be determined. Consequently, creating a formula to determine this number for bonded three-layer structures directly may be the subject of a subsequent paper.
- 4) This paper demonstrates that, for frequencies close to the frequency corresponding to the maximum value of the group velocity of the S0 mode, the adhesive layer thickness has no discernible effect on the mode's group velocity. This is equivalent to a low-frequency region where a horizontal or roughly constant asymptote is admitted by the group velocity curve. Thus, to regulate the adhesive layer quality, this mode is advised.
- 5) It should be mentioned that the dispersion curves are plotted as a cloud of irregularly distributed points if the thickness of the epoxy layer drops below a specific threshold value. Additionally, a large number of the first modes concentrate on a low-frequency band if the thickness is excessively large – and this is practically absurd.

4. CONCLUSION

The purpose of this study was to use the semi-analytical finite element SAFE method to calculate the dispersion curves of ultrasonic guided waves propagating through a bonded planar three-layer structure composed of aluminum, epoxy, and aluminum, and to plot the normalized nodal displacements for the four propagative modes A0, S0, A1, and S1, which appear at the frequency of 200 kHz. The SAFE method was found to be efficient in calculating the dispersion curves for planar bonded three-layer structures and was in good agreement with the GUIGUW program. A second observation given in this paper is that

the A0 mode remains insensitive to the change of the epoxy layer thickness in the low-frequency range; on the other hand, the S0 mode is a good candidate for better testing. If we limit ourselves to the fundamental modes, it appears that the S0 mode is highly recommended for the evaluation and characterization of three-layer structures, and it remains possible to have another mode from the list (A1, S1, A2, S2, etc.) that is more sensitive than the S0 mode for this kind of structure in the low-frequency range.

In general, this paper presents the dispersive behavior of ultrasonic guided waves propagating inside bonded three-layer structures and may be useful in non-destructive testing. This paper showed that for bonded three-layer structures, the number of modes is high compared to that of isotropic single-layer structures, and that the cutoff frequencies of one-order modes, which are A1 and S1, are very close to those of A0 and S0 for the bonded three-layer structures. It has been shown that the S0 mode is very sensitive to changes in the adhesive layer thickness. However, its greater sensitivity is in its most dispersive domain. Then we can use this mode to estimate the difference in epoxy thickness between two supposedly identical structures, one of which is considered a reference based on the difference in phase velocity.

In low frequencies, the S0 mode would be a good choice to examine this kind of structure because of its small dispersive behavior and maximum group velocity. It is shown that the thickness of the adhesive layer has no appreciable effect on the group velocity for frequencies near the frequency corresponding to the maximum value of the group velocity in the S0 mode. This corresponds to a low-frequency region where the group velocity curve admits a horizontal or approximately constant asymptote. Therefore, this mode is recommended to control the quality of the adhesive layer. It should be remembered that for each frequency range, there is a well-defined number of modes, and for all these modes to appear, it is necessary to determine the minimum number of elements from which the maximum number of modes is reached. So, finding a formula to determine this number directly for bonded three-layer structures can be the subject of a future research. Comparing the theoretical findings presented in this paper with experimental findings remains an interesting subject to explore, particularly when attempting to investigate how ultrasonic guided waves interact with a bonding defect.

REFERENCES

1. PILKEY W.D., PILKEY D.F., BI Z., *Peterson's Stress Concentration Factors*, 4th ed., John Wiley & Sons, 2020, doi: 10.1002/9781119532552.
2. LOWE M.J.S., CAWLEY P., The applicability of plate wave techniques for the inspection of adhesive and diffusion bonded joints, *Journal of Nondestructive Evaluation*, **13**(4): 185–200, 1994, doi: 10.1007/BF00742584.

3. CRUSE T.A., VANBUREN W., Three-dimensional elastic stress analysis of a fracture specimen with an edge crack, *International Journal of Fracture Mechanics*, **7**(1): 1–15, 1971, doi: 10.1007/BF00236479.
4. THOMSON W.T., Transmission of elastic waves through a stratified solid medium, *Journal of Applied Physics*, **21**(2): 89–93, 1950, doi: 10.1063/1.1699629.
5. HASKELL N.A., The dispersion of surface waves on multilayered media, *Bulletin of the Seismological Society of America*, **43**(1): 17–34, 1953, doi: 10.1785/BSSA0430010017.
6. SEIFREID R., JACOBS L.J., QU J., Propagation of guided waves in adhesive bonded components, *NDT & E International*, **35**(5): 317–328, 2002, doi: 10.1016/S0963-8695(01)00056-1.
7. LINDGREN E., ALDRIN J.C., JATA K., SCHOLLES B., KNOPP J., Ultrasonic plate waves for fatigue crack detection in multi-layered metallic structures, *Health Monitoring of Structural and Biological Systems, Proceedings of SPIE*, **6532**: 653207, 2007, doi: 10.1117/12.714764.
8. LOWE M.J.S., COWLEY P., The applicability of plate wave techniques for the inspection of adhesive and diffusion bonded joints, *Journal of Nondestructive Evaluation*, **13**(4): 185–200, 1994, doi: 10.1007/BF00742584.
9. ROKHLIN S.I., Lamb wave interaction with lap-shear adhesive joints: theory and experiment, *The Journal of the Acoustical Society of America*, **89**(6): 2758–2765, 1991, doi: 10.1121/1.400715.
10. LOWE M.J.S., CHALLIS R.E., CHAN C.W., The transmission of Lamb waves across adhesively bonded lap joints, *The Journal of the Acoustical Society of America*, **107**(3): 1333–1345, 2000, doi: 10.1121/1.428420.
11. WANG K., LIU M., CAO W., YANG W., SU Z., CUI F., Detection and sizing of disbond in multilayer bonded structure using modally selective guided wave, *Structural Health Monitoring*, **20**(3): 904–916, 2021, doi: 10.1177/1475921719866274.
12. GAUTHIER C., EL-KETTANI M.E.-Ch., GALY J., PREDOI M., LEDUC D., Structural adhesive bonding characterization using guided Lamb waves and the vertical modes, *International Journal of Adhesion and Adhesives*, **98**(3): 102467, 2020, doi: 10.1016/j.ijadhadh.2019.102467.
13. ZITOUNI I., RHIMINI H., CHOUAF A., A combined Newton–Bisection approach for calculating the dispersion curves in anisotropic multilayered waveguides, *Journal of Vibration Engineering & Technologies*, **12**: 5189–5201, 2023, doi: 10.1007/s42417-023-01191-1.
14. ZITOUNI I., RHIMINI H., CHOUAF A., Modeling the propagation of ultrasonic guided waves in a composite plate by a spectral approximation method, *Engineering Transactions*, **71**(2): 213–227, 2023, doi: 10.24423/EngTrans.3073.20230510.
15. ZITOUNI I., RHIMINI H., CHOUAF A., Comparative study of the spectral method, DISPERSSE and other classical methods for plotting the dispersion curves in anisotropic plates, *Journal of Applied and Computational Mechanics*, **9**(4): 955–973, 2023, doi: 10.22055/JACM.2023.42530.3941.
16. NAYFEH A.H., CHIMENTI D.E., Free wave propagation in plates of general anisotropic media, *Journal of Applied Mechanics*, **56**(4): 881–886, 1989, doi: 10.1115/1.3176186.
17. PRIYADARSHINEE P., Calculation of wave dispersion curves in multilayered composites using semi-analytical finite element method, *The Journal of the Acoustical Society of America*, **146**(4_Supplement): 2949–2950, 2019, doi: 10.1121/1.5137244.

18. DENG H., HE Z., CHEN L., Ultrasonic guided wave-based detection of composite insulator debonding, *IEEE Transactions on Dielectrics and Electrical Insulation*, **24**(6): 3586–3593, 2017, doi: 10.1109/TDEI.2017.006665.
19. BOUGAZE B., SIDKI M., RAMDANI A., Guided ultrasonic waves in the tri-layer structures. Application to the non destructive ultrasonic testing of the bonding quality of sheets, *The European Physical Journal-Applied Physics*, **32**(3): 207–212, 2005, doi: 10.1051/epjap:2005090.
20. MEHRABI M., SOORGE M.H., HABIBI H., KAPPATOS V., A novel application of ultrasonic Lamb waves: studying adhesive effects on the inspection of coating debonding in a three-layer waveguide, *Nondestructive Testing and Evaluation*, **36**(6): 616–636, 2021, doi: 10.1080/10589759.2020.1843653.
21. BARTOLI I., MARZANI A., LANZA DI SCALEA F., VIALA E., Modeling wave propagation in damped waveguides of arbitrary cross-section, *Journal of Sound and Vibration*, **295**(3–5): 685–707, 2006, doi: 10.1016/j.jsv.2006.01.021.
22. AHMAD Z.A.B., VIVAR-PEREZ J.M., GABBERT U., Semi-analytical finite element method for modeling of lamb wave propagation, *CEAS Aeronautical Journal*, **4**(1): 21–33, 2013, doi: 10.1007/s13272-012-0056-6.
23. GALÁN J.M., ABASCAL R., Numerical simulation of Lamb wave scattering in semi-finite plates, *International Journal for Numerical Methods in Engineering*, **53**(5): 1145–1173, 2002, doi: 10.1002/nme.331.

Received June 30, 2023; accepted version January 31, 2024.

Online first March 19, 2024.



Copyright © 2024 The Author(s).
Published by IPPT PAN. This work is licensed under the Creative Commons Attribution License
CC BY 4.0 (<https://creativecommons.org/licenses/by/4.0/>).